Applied Radiation and Isotopes 128 (2017) 270–274

Contents lists available at ScienceDirect

Applied Radiation and Isotopes

journal homepage: www.elsevier.com/locate/apradiso

# Tagging fast neutrons from a $^{252}$Cf fission-fragment source

J. Scherzinger[a,b], R. Al Jebali[c], J.R.M. Annand[c], A. Bala[c,1], K.G. Fissum[a,b,*], R. Hall-Wilton[b,d], D. Hamilton[c], N. Mauritzson[a], F. Messi[a,b], H. Perrey[a,b], E. Rofors[a]

[a] Division of Nuclear Physics, Lund University, SE-221 00 Lund, Sweden
[b] Detector Group, European Spallation Source ESS AB, SE-221 00 Lund, Sweden
[c] SUPA School of Physics and Astronomy, University of Glasgow, Glasgow G12 8QQ, Scotland, UK
[d] Mid-Sweden University, SE-851 70 Sundsvall, Sweden

## HIGHLIGHTS

- Neutrons emitted from a $^{252}$Cf source with a thin window are tagged using the corresponding fission fragments.
- The resulting beam of neutrons is continuous and polychromatic.
- The energy of each neutron is determined via the time-of-flight technique.
- The approach is anticipated to facilitate cost-effective determinations of neutron-detector efficiencies.

## ARTICLE INFO

*Keywords:*
Californium-252
Fission fragments
Fast neutrons
Time-of-flight
Tagging

## ABSTRACT

Coincidence and time-of-flight measurement techniques are employed to tag fission neutrons emitted from a $^{252}$Cf source sealed on one side with a very thin layer of Au. The source is positioned within a gaseous $^{4}$He scintillator detector. Together with $\alpha$ particles, both light and heavy fission fragments pass through the thin layer of Au and are detected. The fragments enable the corresponding fission neutrons, which are detected in a NE-213 liquid-scintillator detector, to be tagged. The resulting continuous polychromatic beam of tagged neutrons has an energy dependence that agrees qualitatively with expectations. We anticipate that this technique will provide a cost-effective means for the characterization of neutron-detector efficiency in the energy range 1–6 MeV.

## 1. Introduction

We recently reported on our efforts to "tag" fast neutrons from an $^{241}$Am/$^{9}$Be source (Scherzinger et al., 2015) as the first step towards the development of a source-based fast-neutron irradiation facility. Here, we report on our investigation of a $^{252}$Cf fission-fragment fast-neutron tagging technique very similar to that reported on by Reiter et al. (2006). In contrast to Reiter et al. who employed a thin layer of plastic scintillator to detect the fragments, we use a gaseous $^{4}$He-based scintillator detector with excellent timing characteristics (see below). The corresponding fission neutrons are detected in a NE-213 liquid-scintillator detector. This effort represents our first step towards the development of an apparatus for the measurement of absolute neutron-detection efficiency at our facility.

## 2. Apparatus

### 2.1. Californium fission-fragment source

The actinide $^{252}$Cf is an intense source of fast neutrons. With an overall half life of 2.645 years and a specific activity of 0.536 mCi/μg, it decays by both $\alpha$-particle emission (96.908%) and spontaneous fission (3.092%) (NuDat2). The weighted average $\alpha$-particle energy is ~ 6111.69 keV. The prompt-neutron yield is ~ 3.75 neutrons per fission event (Boldeman and Hines, 1985; Axton and Bardell, 1985). The resulting fast-neutron energy spectrum follows the Watt distribution (Fröner, 1990) and is very well known, with a most-probable energy of 0.7 MeV and an average energy of 2.1 MeV. Our californium source (Eckert & Ziegler) has an active diameter of 5 mm and is mounted in a capsule that has a thick platinum-clad nickel back side and a thin 50 μg/cm$^2$ sputtered-gold front side which allows both $\alpha$ particles and fission fragments to escape. The (nominal) activity is 3.7 MBq. While

* Corresponding author at: Division of Nuclear Physics, Lund University, SE-221 00 Lund, Sweden.
*E-mail address:* kevin.fissum@nuclear.lu.se (K.G. Fissum).
[1] Present address: Usmanu Danfodiyo University, Sokoto, Nigeria.

http://dx.doi.org/10.1016/j.apradiso.2017.05.022
Received 5 December 2016; Received in revised form 16 May 2017; Accepted 28 May 2017
Available online 30 May 2017

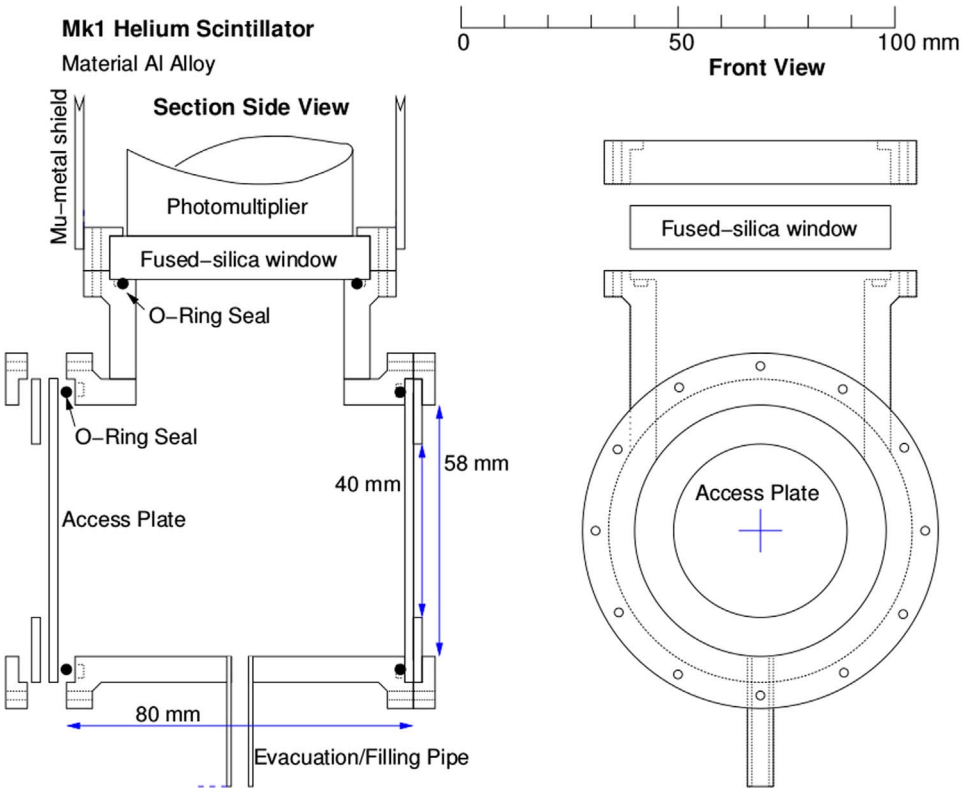


**Fig. 1.** A drawing of the gas cell. Left panel: Section Side View. The cell is filled with 5 bar of gaseous $^4$He scintillator and 500 ppm gaseous $N_2$ wavelength shifter. Right panel: Front View. The photomultiplier tube is attached via a fused-silica window from the top.

trace activity comes from $^{249}$Cf (<0.2%) and $^{251}$Cf (<0.04%), the majority comes from $^{250}$Cf (~ 7.5%) and $^{252}$Cf (~ 92.3%). We estimate a neutron emission rate of ~ $4 \times 10^5$ neutrons per second.

### 2.2. Gaseous $^4$He fission-fragment detector

The noble gas $^4$He is a good scintillator with an ultra-violet light yield of about the same magnitude as intrinsic (non Tl-doped) NaI crystals (Birks et al., 1964; Dolgosheim et al., 1969; Knoll, 1989; Aprile et al., 2006). In this measurement, we employed a gas cell built originally as a prototype active target for recent $^4$He photoreaction measurements (Al Jebali et al., 2015). The cell was machined from a solid aluminum block and has a cylindrical interior volume measuring 72 mm long × 58 mm $\phi$, for an inner volume of ~ 0.19 liters (see Fig. 1).

The interior of the gas cell was sandblasted and then treated with two layers of water soluble EJ-510 reflective paint. A fused-silica optical window 10 mm thick × 60 mm $\phi$ is pressed against the body of the cell and allows the scintillation light produced by the $\alpha$ particles and fission fragments to escape. A rubber O-ring provides the pressure seal. The cell was filled with 5 bar 99.99999% pure $^4$He (scintillator) gas together with 2.5 mbar 99.99999% pure $N_2$ (scintillation-wavelength shifter) gas. With this very small concentration, the $N_2$ dopant resulted in visible scintillations appropriate for a photomultiplier tube (PMT) that were very fast, having risetimes of a few ns and falltimes of a few 10s of ns. A photograph of the assembled cell is shown in the left panel of Fig. 2. A 5.08 cm XP2262B photomultiplier tube was attached to the optical window and EJ-550 optical grease was employed at the boundary. A photograph of the assembled detector (gas cell and PMT) is shown in the right panel of Fig. 2.

The californium source described above was positioned at the center of the gas cell so that the thin front side through which the $\alpha$ particles and fission fragments could escape faced away from the PMT. The distance from the californium source to the center of the fused-silica optical window was ~ 65 mm. The operating voltage for the PMT was −1750 V and the discriminator threshold was set at −60 mV. Typical signal risetime was 5 ns, while the falltime to <10% of the original amplitude was ~ 10 ns. Fig. 3 shows some typical detector pulses obtained with the $^4$He gas cell. The top traces with amplitudes of about −350 mV correspond to $\alpha$ particles. The middle traces with amplitudes of about −1600 mV correspond to heavy fission fragments. The bottom traces with amplitudes of about −2200 mV correspond to light fission fragments. We note that the average $\alpha$-particle energy is ~ 6.1 MeV, while the average heavy fission-fragment energy is 80 MeV and the


**Fig. 2.** Fission-fragment detector. Left panel: photograph of the $^4$He gas cell. The painted interior of the cell is visible (white). The photomultiplier (PMT) tube mounts from the top. Right panel: photograph of the gas cell and PMT assembly. The assembly as been rotated and the now-mounted PMT corresponds to the black cylinder to the right. (For interpretation of the references to color in this figure caption, the reader is referred to the web version of this article).

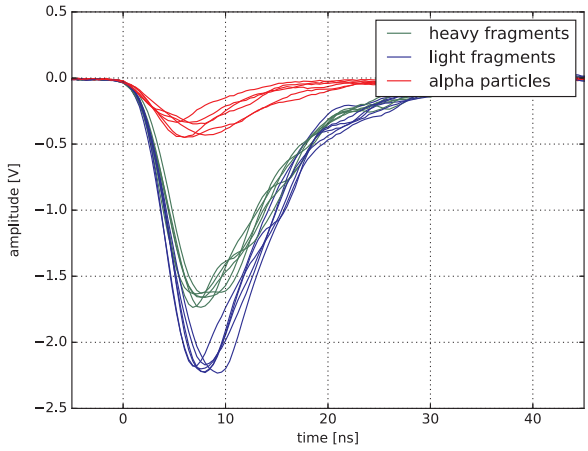


**Fig. 3.** Typical pulses associated with the decay of $^{252}$Cf obtained with the $^{4}$He gas cell. Top (red) trace: $\alpha$ particles. Middle (green) trace: heavy fission fragments. Bottom (blue) trace: light fission fragments. (For interpretation of the references to color in this figure caption, the reader is referred to the web version of this article).

**Fig. 4.** The NE-213 detector (CAD representation). Top: the aluminum scintillator "cup" which holds the NE-213. A (light brown) window separates the scintillator from the lightguide. Bottom: The "cup" is to the left. The $\mu$-metal shielded PMT and base assembly is the black cylinder to the right. Figure from Jebali (2015). (For interpretation of the references to color in this figure caption, the reader is referred to the web version of this article).

average light fission-fragment energy is 104 MeV (van Aarle et al., 1994).

### 2.3. NE-213 fast-neutron and gamma-ray liquid-scintillator detector

NE-213 is an organic liquid scintillator that has been employed for decades as a fast-neutron detector. The NE-213 liquid-scintillator detector used here (Fig. 4) has been reported upon earlier (Scherzinger et al., 2015; Jebali et al., 2015; Scherzinger et al., 2016). It consisted of a 62 mm long × 94 mm $\phi$ cylindrical aluminum "cup" fitted with a borosilicate glass optical window (Glasteknik). The filled cell was dry-fitted against a cylindrical UVT lightguide (Poly(methyl-methacrylate), PMMA) and coupled to a $\mu$-metal shielded 7.62 cm ET 9821KB PMT and base (ET Enterprises). The operating voltage was set at about −1900 V, and the energy calibration was determined using standard gamma-ray sources together with a slightly modified version of the method of Knox and Miller (1972) as described in Scherzinger et al. (2016). The detector threshold was set at 150 keV electron equivalent (keV$_{ee}$), corresponding to a neutron depositing an energy of about 1 MeV.

### 2.4. Configuration

A block diagram of the electronics is shown in Fig. 5. $\alpha$ particles and fission fragments were detected in the $^{4}$He scintillator detector and

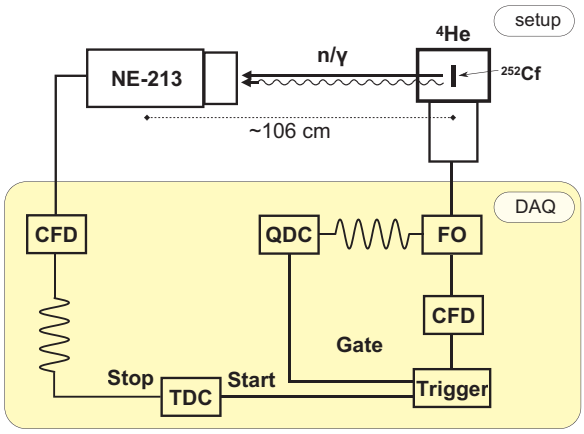


**Fig. 5.** A simplified overview of the experimental setup (not to scale). The $^{4}$He scintillator detector (which contains the $^{252}$Cf source) and the NE-213 detector are shown together with a block electronics diagram (yellow box) illustrating the time-of-flight concept employed. (For interpretation of the references to color in this figure caption, the reader is referred to the web version of this article).

corresponding neutrons (and gamma-rays) were detected in the NE-213 detector. The analog signals from the NE-213 detector were passed to a Phillips Scientific (PS) 715 NIM constant-fraction timing discriminator (CFD). The analog signals from the $^{4}$He scintillator detector were fanned out (FO) and passed to a PS 715 NIM CFD as well as a CAEN V792 12-bit (DC-coupled 60 ns gate) VME QDC. The CFD signals from the $^{4}$He scintillator detector were used to trigger the data acquisition (DAQ) and thus provided start signals for a CAEN 1190B VME multihit time-to-digital converter (TDC) used for the neutron time-of-flight (TOF) determination. The NE-213 detector provided the corresponding stop signal. A SIS 1100/3100 PCI-VME bus adapter was used to connect the VMEbus to a LINUX PC-based DAQ system. The signals were recorded and processed using ROOT-based software (Brun and Rademakers, 1997).

## 3. Results

Fig. 6 shows a deposited-energy spectrum measured using the $^{4}$He scintillator detector. The top panel is plotted on a logarithmic scale to better illustrate the overall features of the spectrum, while the bottom panel is plotted on a linear scale to emphasize certain of these features. The very sharp leftmost peak in the figure located at about channel 80 is the pedestal or zero-energy bin in the QDC. Just to the right of the pedestal is the edge corresponding to our hardware threshold located at about channel 140. Recall that this discriminator threshold was −60 mV. The $\alpha$ particles which dominate the spectrum and correspond to the red trace in Fig. 3 correspond to the peak centered at about channel 190. Note that our energy resolution at this energy is about 50%, so that the entire $\alpha$-particle distribution is not shown as the hardware threshold cuts into it. A distribution corresponding to heavy fission fragments (green trace in Fig. 3) is shown here centered at channel 950, while that corresponding to light fission fragments (blue trace in Fig. 3) is centered at channel 1310. Separation of fission fragments and $\alpha$ particles is not completely clean, as seen in the grey shaded area of Fig. 6 between channels 230 and 540. This could result from non-uniform scintillation-light collection, different energy losses of different particle types in the source as well as the thin Au source window, non-linearity of the scintillation, or even fission fragments striking the source holder. This will be examined in more detail in a future publication. Recall that the average $\alpha$-particle energy is ~ 6.1 MeV, while the average heavy fission-fragment energy is 80 MeV and the average light fission-fragment energy is 104 MeV. If we calibrate our QDC based upon the average energy deposition of the two types of fission fragments and then apply this calibration to the

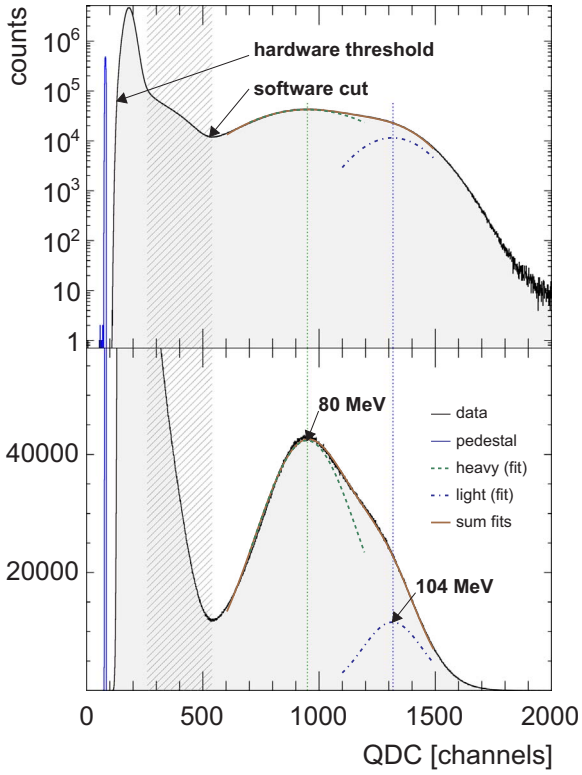


**Fig. 6.** Deposited-energy histogram measured using the $^4$He fission-fragment detector. Both panels present the same data set. The pedestal (leftmost blue peak), hardware discriminator threshold, software fission-fragment cut, and distributions corresponding to $\alpha$-particles (dominant peak), heavy fission fragments (green dashed line), and light fission fragments (blue dot-dashed line) are all shown. (For interpretation of the references to color in this figure caption, the reader is referred to the web version of this article).

$\alpha$-particle distribution, we reconstruct the $\alpha$ peak at $\sim$ 12 MeV. $^4$He is often assumed to be a linear scintillator, while this preliminary analysis suggests an apparent non-linearity. However, as outlined above, there are several factors which will affect this apparent non-linearity in the scintillation-pulse height including the lower-energy portion of the $\alpha$-particle distribution being eliminated by the discriminator threshold. The degree of non-linearity in the scintillation (if any) requires an in-depth study. Note that for the data presented subsequently in this paper, a software fission-fragment cut located at channel 520 was employed.

Fig. 7 shows a fission-neutron TOF spectrum obtained using the signal in the $^4$He scintillator detector to start a TDC and a signal from the NE-213 detector to stop it. Note that the spectrum shown corresponds to events lying above the software fission-fragment cut at

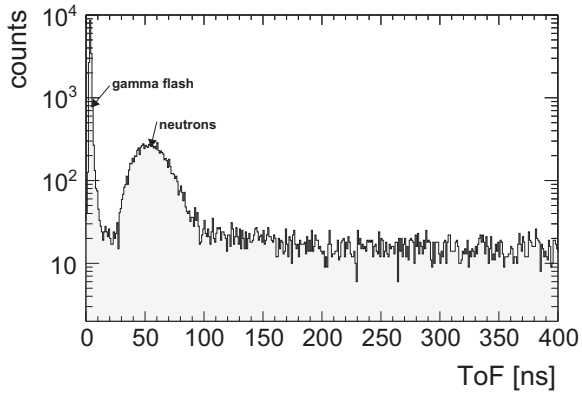


**Fig. 7.** Fission-neutron TOF spectrum. The gamma-flash and fission-neutron distribution are shown. The flat background is due to random events.

channel 520 shown in Fig. 6. After this cut, interpretation of the resulting TOF spectrum is straightforward. The sharp peak to the left of the spectrum centered at about 5 ns and labeled “gamma-flash” corresponds to the detection of a fission fragment in the $^4$He scintillator detector and a correlated fission-event gamma-ray in the NE-213 detector. The $\sim$ 1.8 ns FWHM of the gamma-flash distribution is consistent with the observed timing jitter on our PMT signals and the slight tail in the distribution is possibly due to time walk in the electronics. Note that $^4$He scintillator is highly insensitive to gamma-rays (Al Jebali et al., 2015; Jebali et al., 2015) and any electrons produced via Compton scattering or pair production will result in only a very small scintillation signal. These events will be entirely suppressed by the relatively high software cut we have applied on the signals from the $^4$He fission-fragment detector. Thus, the present apparatus is almost completely insensitive to fission-associated multiple gamma-ray events. The broad bump centered at about 55 ns corresponds to the fission-neutron distribution. The underlying background distribution corresponds to random coincidences. It was measured to be flat as expected by breaking the line-of-sight between the $^4$He scintillator detector and the NE-213 detector using a stack of lead ($\sim$ 15 cm) and polyethylene ($\sim$ 10 cm).

Fig. 8 shows the measured fission-neutron TOF spectrum from Fig. 7 converted to a neutron kinetic-energy spectrum together with three representations of the neutron kinetic-energy distribution constructed using the information presented in Thomas (2014). To convert from TOF to neutron kinetic energy, we used the $\sim$ 5 ns position of the gamma-flash shown in Fig. 7 and the 106 cm distance between the $^{252}$Cf source and the center of the NE-213 liquid-scintillator cell. The data were then rebinned linearly in kinetic energy. We note that there are small differences between the representations of the neutron kinetic-energy distributions, so a different normalization factor has been applied to each so that they exactly coincide with our data at 1.5 MeV. It should be emphasized that the present data have not been corrected in any way for such effects as neutron-detection efficiency. Instead, we stress that the shape of our measured distribution agrees qualitatively with that which is expected. This indicates that we are tagging neutrons. Ultimately, comparing such tagged-neutron spectra after they have been corrected for effects such as the scattering of neutrons into the detector to the expected neutron kinetic-energy distributions will enable neutron-detection efficiency to be quantified. However, with the present hardware neutron-detector threshold, detection efficiencies for neutrons with energies below 1 MeV will not be measurable.

At 1.5 MeV, the agreement between all three representations of the

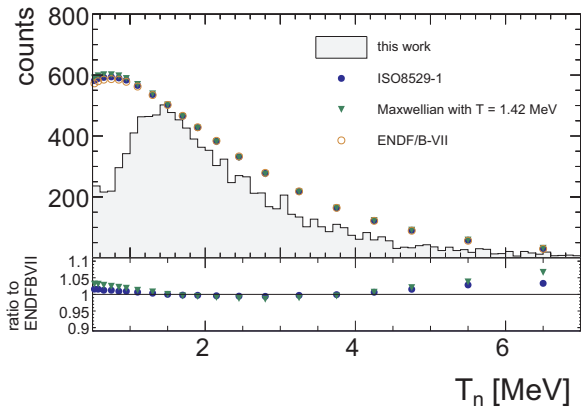


**Fig. 8.** Fission-neutron kinetic-energy spectra for $^{252}$Cf. Top panel: The grey histogram is measured data. Also shown are the ISO 8529-1 recommendation (filled blue circles), a Maxwellian approximation (green triangles), and the ENDF/B-VII suggestion (open red circles) for the fission-neutron spectrum. Bottom panel: The ratio of the ISO 8529-1 recommendation (filled blue circles) and a Maxwellian approximation (green triangles) to the ENDF/B-VII suggestion. (For interpretation of the references to color in this figure caption, the reader is referred to the web version of this article).

neutron kinetic-energy distributions is essentially exact. This very good agreement continues up to 4 MeV, as the Maxwellian approximation and the ISO 8529-1 representation both lie below the ENDF/B-VII suggestion by less than 2% and 1%, respectively. By 4.5 MeV, the agreement between all three is again essentially exact. Above 6 MeV, a divergence between the representations begins and by 6.5 MeV, both the Maxwellian and the ISO 8529-1 representations lie above the ENDF/B-VII suggestion by about 7% and 3%, respectively. This divergence increases with energy, and by 8 MeV, the ratios are 9% and 4%, respectively. The ± 1% level of agreement between all three representations of the $^{252}$Cf fission-neutron energy spectrum over the energy region from 1 to 6 MeV is well within any systematic uncertainty that we are likely to obtain in measurements of neutron-detection efficiency using the tagging technique presented here. Thus, they provide an excellent benchmark from which it will be possible to evaluate neutron-detection efficiency.

Our next step will be to optimize the parameters of the proof-of-principle measurement put forth in this article to establish a benchmark TOF configuration. In conjunction with measurements in this benchmark configuration, we will simulate the detector response and neutron-detection efficiency using GEANT4 (Agostinelli et al., 2003; Allison et al., 2006) and MCNP to establish our absolute knowledge of our neutron beam in this configuration. Knowledge of the neutron beam in this configuration will facilitate the subsequent understanding of the responses of other detectors investigated using exactly this setup.

## 4. Summary

As a first step towards the development of an apparatus for the measurement of neutron-detection efficiency at our source-based fast-neutron irradiation facility, we have employed coincidence and time-of-flight measurement techniques to “tag” neutrons emitted by a $^{252}$Cf source. The spontaneous-fission fragments are detected in a gaseous $^{4}$He scintillator detector. The neutrons are detected in a NE-213 liquid-scintillator detector. The resulting continuous polychromatic beam of tagged neutrons has a measured energy dependence that agrees qualitatively with expectations. This preliminary study strongly suggests that the method of neutron-energy tagging will work well and future investigations will concentrate on quantifying systematic effects in order to optimize the performance. We anticipate that the technique will provide a cost-effective means for the characterization of neutron-detector efficiency, and note that this technique will work equally well for all spontaneous-fission neutron sources.

## Acknowledgements

We acknowledge the support of the UK Science and Technology Facilities Council (Grant nos. STFC 57071/1 and STFC 50727/1) and the European Union Horizon 2020 BrightnESS Project, Proposal ID 676548.

## References

Agostinelli, S., et al., 2003. Nucl. Instrum. Methods Phys. Res. A 506, 250. http://dx.doi.org/10.1016/S0168-9002(03)01368-8.
Al Jebali, R., et al., 2015. Eur. Phys. J. A 51, 123. http://dx.doi.org/10.1140/epja/i2015-15123-y.
Allison, J., et al., 2006. IEEE Trans. Nucl. Sci. 53, 270. http://dx.doi.org/10.1109/TNS.2006.869826.
Aprile, E., Bolotnikov, A.E., Bolozdynya, A.I., Doke, T., 2006. Scintillation detectors, In: Noble Gas Detectors. Wiley-VCH Verlag GmbH, KGaA, Weinheim Germany, ISBN: 978-3-527-40597-8.
Axton, E.J., Bardell, A.G., 1985. Metrologia 21, 59.
Birks, J.B., Fry, D.W., L Costrell, K Kandish, K, The Theory and Practice of Scintillation Counting, Pergamon Press, New York, U.S.A., 1964, ISBN: 978-0-08-010472-0.
Boldeman, J.W., Hines, M.G., 1985. Nucl. Sci. Eng. 91, 114.
Brun, R., Rademakers, Fons, 1997. In: Proceedings of the AIHENP'96 Workshop. Lausanne, Sep. 1996. Nucl. Instrum. Methods in Phys. Res. A 389, 81–86. See also ⟨https://root.cern.ch/⟩.
Dolgosheim, B.A., Rodionov, B.U., 1969. The mechanism of noble gas scintillation. In: Elementary Particles and Cosmic Rays. Volume 2, Atomizdat, Moscow Russia.
Eckert & Ziegler. Supplied by Eckert & Ziegler Isotope Products GmbH. Activity: Testing performed 1 April 2015 at Eckert & Ziegler Isotope Products Medical Imaging Laboratory, 24937 Avenue Tibbitts, Valencia CA 91355, USA.
EJ-510. ⟨http://www.eljentechnology.com/products/accessories/ej-510-ej-520⟩.
EJ-550. ⟨http://www.eljentechnology.com/images/products/data_sheets/EJ-550_EJ-552.pdf⟩.
ET Enterprises. ⟨http://www.et-enterprises.com/files/file/Pmtbrochure11.pdf⟩ for details.
Fröner, F.H., 1990. Nucl. Sci. Eng. 106, 345.
Glasteknik. ⟨http://www.us.schott.com/borofloat/english⟩ for details. Supplied by Glasteknik i Emmaboda AB, Utvägen 6 SE-361 31 Emmaboda, Sweden.
Jebali, R., et al., 2015. Nucl. Instrum. Methods Phys. Res. A 794, 102. http://dx.doi.org/10.1016/j.nima.2015.04.058.
Knoll, G.F., 1989. Radiation Detection and Measurement. Wiley, New York, U.S.A., ISBN: 9780471815044, ⟨http://books.google.com/books?id=dyBRAAAAMAAJ⟩.
Knox, H.H., Miller, T.G., 1972. Nucl. Instrum. Methods 101, 519.
NE-213 is no longer produced. Eljen Technologies offers EJ-301 ⟨http://www.eljentechnology.com/images/products/data_sheets/EJ-301_EJ-309.pdf⟩ while Saint Gobain offers BC-501 ⟨http://www.crystals.saint-gobain.com/sites/imdf.crystals.com/files/documents/sgc-bc501-501a-519-data-sheet_69711.pdf⟩.
NuDat2. ⟨http://www.nndc.bnl.gov/nudat2/⟩.
MCNP: See ⟨https://mcnp.lanl.gov/⟩ and ⟨https://laws.lanl.gov/vhosts/mcnp.lanl.gov/pdf_files/la-ur-03-1987.pdf⟩ for details.
Poly(methyl-methacrylate), also known as Acrylic, Plexiglass, and Lucite. Supplied by Nordic Plastics Group AB, Bronsyxegatan 6, SE-213 75 Malmö, Sweden.
Reiter, A., et al., 2006. Nucl. Instrum. Methods Phys. Res. A 565, 753. http://dx.doi.org/10.1016/j.nima.2006.06.048.
Scherzinger, J., et al., 2015. Appl. Radiat. Isot. 98, 74. http://dx.doi.org/10.1016/j.apradiso.2015.01.003.
Scherzinger, J., et al., 2016. Nucl. Instrum. Methods Phys. Res. A 840, 121. http://dx.doi.org/10.1016/j.nima.2016.10.011.
Thomas, D., 2014. ESARDA Bull. 51, 45.
van Aarle, J., et al., 1994. Nucl. Phys. A578, 77. http://dx.doi.org/10.1016/0375-9474(94)90970-9.
XP2262B. ⟨https://my.et-enterprises.com/pdf/XP2262.pdf⟩.